JOURNAL OF GEOPHYSICAL RESEARCH, VOL. 93, NO. B11, PAGES 13,307-13,318, NOVEMBER 10, 1988

The Growth of Geological Structures by Repeated Earthquakes

1. Conceptual Framework

GEOFFREY C. P. KING

U.S. Geological Survey, Denver, Colorado

ROSS S. STEIN

U.S. Geological Survey, Menlo Park, California

JOHN B. RUNDLE

Sandia National Laboratories, Albuquerque, New Mexico

In many places, earthquakes with similar characteristics have been shown to recur. If this is common, then relatively small deformations associated with individual earthquake cycles should accumulate over time to create geological structures. Following this paradigm, we show that existing models developed to describe leveling line changes associated with the seismic cycle can be adapted to explain geological features associated with a fault. In these models an elastic layer containing the fault overlies a viscous half-space with a different density. Fault motion associated with an earthquake results in immediate deformation followed by a long period of readjustment as stresses relax in the viscous layer and isostatic equilibrium is restored. Deformation is also caused as a result of the loading and unloading due to sediment deposition and erosion. In this paper, the parameters that control the growth of dip-slip structures are identified. We find that the flexural rigidity of the crust (or the apparent elastic thickness) provides the main control of the width of a structure. The loading due to erosion and deposition of sediment determines the ratio of uplift to subsidence between the two sides of the fault. The flexure due to sediment load is much more important in this respect than whether the fault is normal or reverse in character. We find that, in general, real structures are associated with apparent elastic thicknesses of 4 km or less and thus with very low flexural rigidities.

INTRODUCTION

We explore here and in an accompanying paper [*Stein* et al. this issue; hereafter Paper 2] the concept that basins and ranges bounded by active faults evolve by sudden deformation during large earthquakes, and by slow deformation between the earthquakes. This paper considers the geometrical concepts involved and provides idealized examples, while the second paper adopts these concepts to consider specific field examples.

Reid [1910] argued that, for great strike-slip earthquakes, seismic and interseismic deformations are nearly equal in magnitude and opposite in sign and thus result in no permanent deformation except for the offset at the fault. We suggest that this interpretation is generally untrue because of the effects of finite fault dimensions, ductility and gravitational forces. The seismic and interseismic deformation do not entirely cancel but accumulate to form permanent structures. The processes are particularly clear for the dip-slip earthquakes that we examine in this study. Comparable techniques can be applied to strike-slip fault systems (R. G. Bilham and G. C. P. King, The influence of fault zone geometry and non uniform slips on the geopraphic expression of strike-slip faults: Examples from the San Andreas Fault, California, submitted to *Journal of Geophysical Research*, 1988) although the structures created are less dramatic.

At the boundaries of oceanic plates, where great earthquakes can repeat at 100-year intervals, the seismic and interseismic deformation have been directly measured landward of the trench. Within continents, where deformation becomes distributed, large normal or reverse faulting earthquakes repeat at much longer periods, and the complete interseismic deformation cannot possibly be measured in the foreseeable future [*Wallace*, 1984]. However, the geological structures that result from many cycles can be predicted on the basis of our understanding of interseismic processes and used to investigate both these processes and the nature of the geological structures themselves.

A model similar to the one that we adopt was originally proposed by *Rundle* [1982a]; it has also been used by other authors [*Thatcher and Rundle*, 1979; *Thatcher*, 1984; *Savage and Gu*, 1985]. In their studies, post earthquake deformation is considered to result from the partial relaxation of stresses set up in the crust by the earthquake. These stresses result from both elastic deformation and gravitational forces. The principal difference between our model and theirs is that we also include the crustal flexure due to the erosion and deposition of sediment. This is summarized in Figure 1.

Paper number 88JB03293.

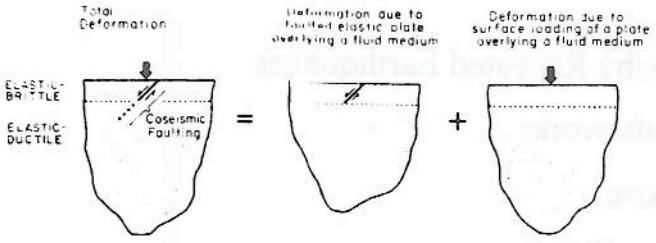

Fig. 1. Deformation due to faulting in the crust. The final deformation is the sum of that due to faulting in a gravitating elastic plate overlying a fluid medium and the surface loading on the same system due to erosional loading and unloading. The faulting that accompanies earthquakes can extend well into the underlying elastic-ductile medium. However, if this region behaves in the long term like a fluid, then this feature of coseismic behavior leaves no trace in the surface rocks or structures. The model does not consider shallow processes that create surface folds [*Stein and King*, 1984]; we are concerned with modeling longer wavelength features that are the surface reflection of deeper processes.

Although deformation can occur by surface loading, such deformation scarcely seems significant within a single earthquake cycle. Viewed over a longer period of time, however, it clearly cannot be ignored. If the material eroded from an uplifted range simply fills the adjacent basin, then flexure occurs because the surface load is moved. More commonly, however, the barrier created by a structure traps sediment transported by rivers over great distances, resulting in a net build up of the load. Alternatively, an overall loss of load is possible, and surprisingly large uplifts can occur.

Crustal deformation resulting from the addition or removal of surface loads has been well studied. For example, uplift associated with the shrinking of Lake Bonneville has been re-examined by *Bills and May* [1987], and Fennoscandian uplift following glaciation was re-evaluated by *Cochran* [1980]. Similarly, the loading within large sedimentary basins was discussed recently by *Watts et al.* [1982]. Such studies produce estimates of the flexural rigidity of the crust (commonly described by an effective elastic thickness) that range from 5 to 25 km. Flexural rigidity has also been examined by comparing gravitational profiles with topographic profiles. The method involves producing a filter $Q(x)$ that, when convolved with the topography $H(x)$, produces the gravity $G(x)$, where $G(x)=Q(x) * H(x)$. The filter so determined is then compared with theoretical filters generated for various models. The method usually assumes that topography and gravity anomalies result solely from loads placed on the surface, although alternative explanations have been considered [*Rundle*, 1982*b*; *Forsyth*, 1985]. Instead of examining the admittance function $Q(x)$, some authors now prefer to examine the coherence between $G(x)$ and $H(x)$. Whatever technique is adopted, values for effective elastic thickness are generally small compared with those derived from studies of loading flexure. For tectonically active parts of the western United States, values range from 4 to 8 km [*Forsyth*, 1985]; much less than the depth range over which small earthquakes occur [e.g., *Sibson*, 1982]. Here, we also find low values for flexural rigidity. These follow as a direct consequence of a simple, general observation which is independent from other approaches. Coseismic deformation observed geodetically occurs over a zone comparable in width with geological structures associated with an active fault. If creep occurs only below the depth to which an earthquake ruptures, then the long-term structures produced by repeating earthquakes would be much wider than those observed. Only by allowing the crust to have long-term strength over a smaller depth range can the conundrum be resolved.

COSEISMIC AND POSTSEISMIC DEFORMATION

As a first approximation, the deformation in an seismic cycle is that which occurs at the time of the earthquake, the coseismic deformation [*King and Brewer*, 1983; *Stein and King*, 1984; *Vita-Finzi and King*, 1985]. Such models adequately describe small features, such as surface folds or footwall folds, but large features cannot be modeled.

A more realistic model was developed by *Rundle* [1982*a*] to explain deformation in the seismic cycle. An upper layer containing the earthquake fault retains strength indefinitely and acts elastically, but the material beneath relaxes stress at a rate determined by its viscosity. Thus, deformation changes with time following the earthquake. The procedure to calculate surface deformation for such a model was described in detail by *Rundle* [1980], who adopted the Thomson-Haskell (propagator) matrix method to first calculate the response of a layered elastic medium to an embedded dislocation source of arbitrary orientation. To fully incorporate the effects of gravitation, 6x6 matrices are required. *Rundle* [1981], however, showed that these can be reduced to 4x4 matrices for a flat layered model because the effect of the gravitational gradient is negligible. The resulting Green's functions are integrated analytically to provide the response due to a fault of finite extent.

The propagator matrix method is quite general and can be used to calculate the time dependent effects from one or more viscoelastic, or viscous, layers. Displacements, stresses, and strains are decomposed by means of Fourier-Bessel transforms in space, so that physical quantities are functions of the Fourier wave number k only. Elastic properties, such as modulii, are replaced by the Laplace transforms of the viscoelastic relaxation functions. Inversion back to the space-time domain is accomplished by means of inverse Fourier-Bessel and Laplace transforms. Although inverse Laplace transforms are, in principle, complicated by the existence of poles and branch cuts in the complex s plane, stable results can nevertheless be obtained by numerical methods [see *Rundle*, 1982a]. For the purposes of this study we evaluate deformation at t=0 and for very large t.

The parameters controlling the major features of the Rundle model can be seen by using example calculations. Figure 2 shows the vertical displacements due to a fault extending to a depth, H, of 16 km in a uniform elastic half-space, and those that remain for the same fault when all stress is relaxed below a depth of 16 km. Figure 2a shows the vertical displacements for a thrust fault and Figure 2*b* for a normal fault. For faults dipping at 45°, the only difference between the displacements, and hence the strains and stresses, between a normal and a reverse fault is the sign. Thus in the absence of the effects of loading, generalizations about normal fault relaxation processes

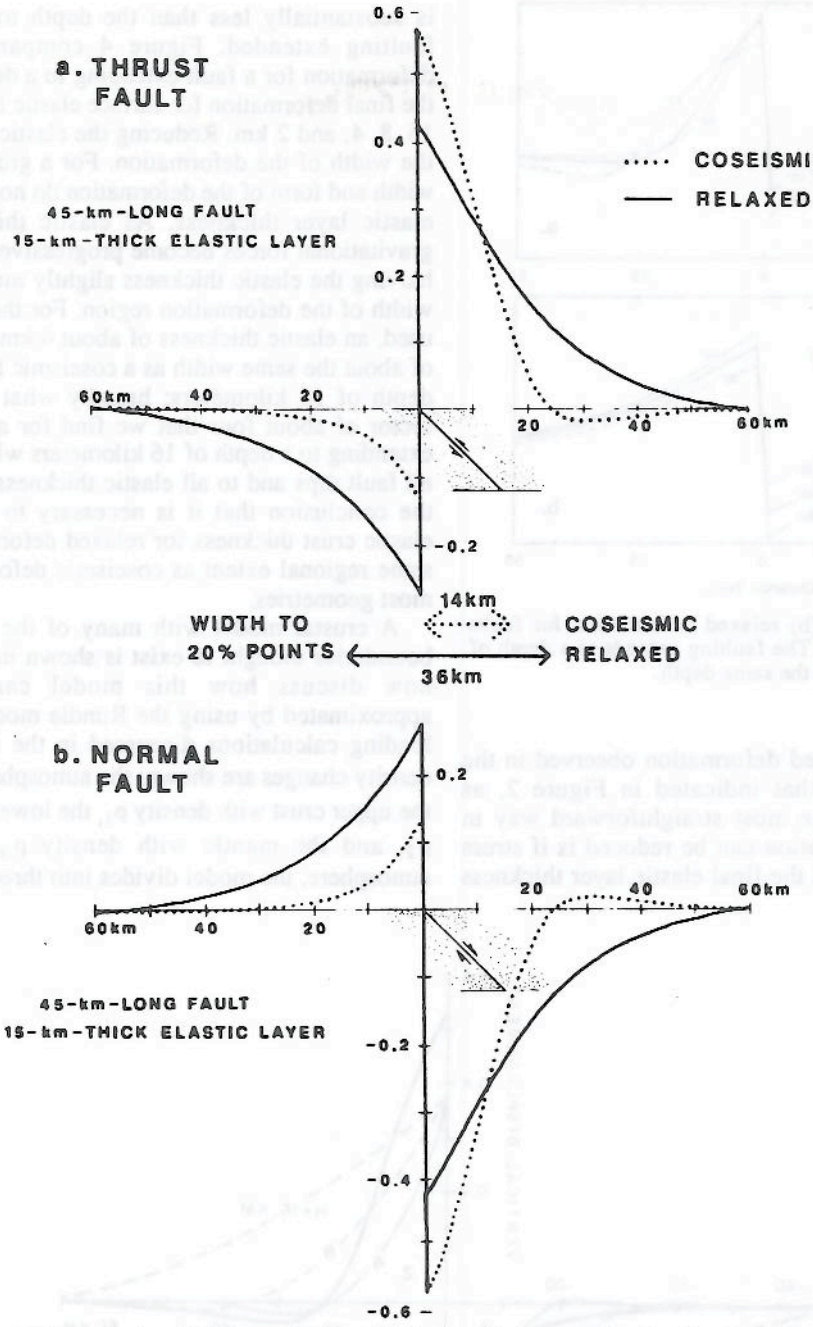

Fig. 2. Coseismic and relaxed deformation for 45° dipping faults associated with no erosion and deposition. Note that the deformation for a normal fault can be found by reversing the sign of fault slip for a thrust fault. All vertical displacements change sign in the same way. Coseismic faulting extends to a depth of 15 km; stress is relaxed below this depth to represent interseismic processes. A 15-km-thick elastic layer causes the relaxed deformation to spread over a width (W) of 36 km much wider than the coseismic deformation (W=14 km). This effect is not observed in real structures.

apply equally to reverse faults. Two features are evident from the models. First, whereas a large difference exists between the amount of uplift and subsidence at the time of an earthquake, they are similar when stress has been relaxed at depth. Second, the width over which deformation extends is greater after stress is relaxed at depth than immediately following the earthquake. For convenience, we define the width, W, of the deformation to be the horizontal dimension normal to the fault strike where the uplift or subsidence is greater than 20% of the vertical offset at the fault.

The effect of changing the dip of the fault is shown in Figure 3. Coseismic deformation associated with faults dipping at 30°, 45° and 60° are shown in Figure 3*a*. The vertical displacements are normalized to 1 m of dip-slip motion with the conseqence that the vertical offset is less for the 30° than for the 60° dipping faults. Figure 3*b* shows the deformation when stress is relaxed at a depth of 15 km. These profiles differ mainly in total offset and very little in form. We conclude that the models in this paper and *Paper 2* are not sensitive to restricting our calculations to 45° dipping faults.

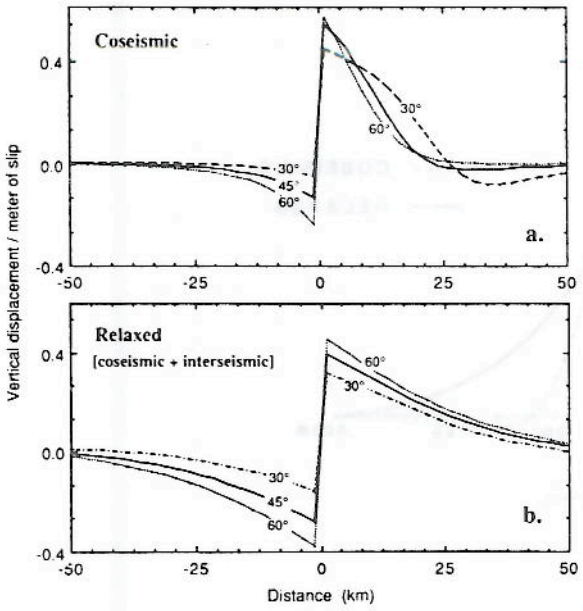

Fig. 3. (a) Coseismic and (b) relaxed deformation for faults dipping at 30°, 45°, and 60°. The faulting extends to a depth of 15 km and stress is relaxed at the same depth.

The width of the relaxed deformation observed in the field is much less than that indicated in Figure 2, as illustrated in *Paper 2*. The most straightforward way in which the relaxed deformation can be reduced is if stress relaxation occurs such that the final elastic layer thickness is substantially less than the depth to which coseismic faulting extended. Figure 4 compares the coseismic deformation for a fault extending to a depth of 16 km with the final deformation for surface elastic layer thicknesses of 16, 8, 4, and 2 km. Reducing the elastic thickness narrows the width of the deformation. For a gravitating model the width and form of the deformation do not exactly scale with elastic layer thickness. As elastic thickness decreases, gravitational forces become progressively more important; halving the elastic thickness slightly more than halves the width of the deformation region. For the 45° dipping fault used, an elastic thickness of about 4 km produces a profile of about the same width as a coseismic fault extending to a depth of 16 kilometers; broadly what is observed. This factor of about four that we find for a 45°-dipping fault extending to a depth of 16 kilometers will not generalize to all fault dips and to all elastic thickness ranges. However, the conclusion that it is necessary to thin the effective elastic crust thickness for relaxed deformation to have the same regional extent as coseismic deformation is true for most geometries.

A crustal model with many of the material property boundaries thought to exist is shown in Figure 5; we will now discuss how this model can be reasonably approximated by using the Rundle model plus the simple loading calculations discussed in the next section. Four density changes are shown: the atmosphere with density ρ_0, the upper crust with density ρ_1, the lower crust with density ρ_2, and the mantle with density ρ_3. Apart from the atmosphere, the model divides into three types of material.

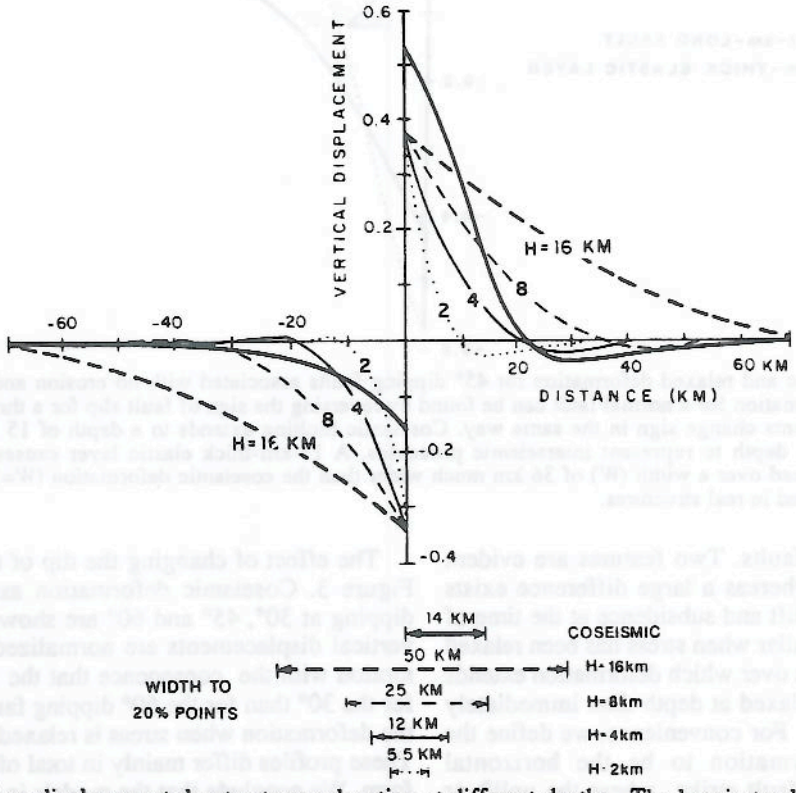

Fig. 4. Surface displacement due to stress relaxation at different depths. The heaviest solid line shows the coseismic deformation for faulting extending to a depth of 16 km. Other lines show the deformation resulting from relaxing stress at depths (H) less than 16 km. The width (W, defined in the text) over which the relaxed deformation occurs narrows as H is reduced.

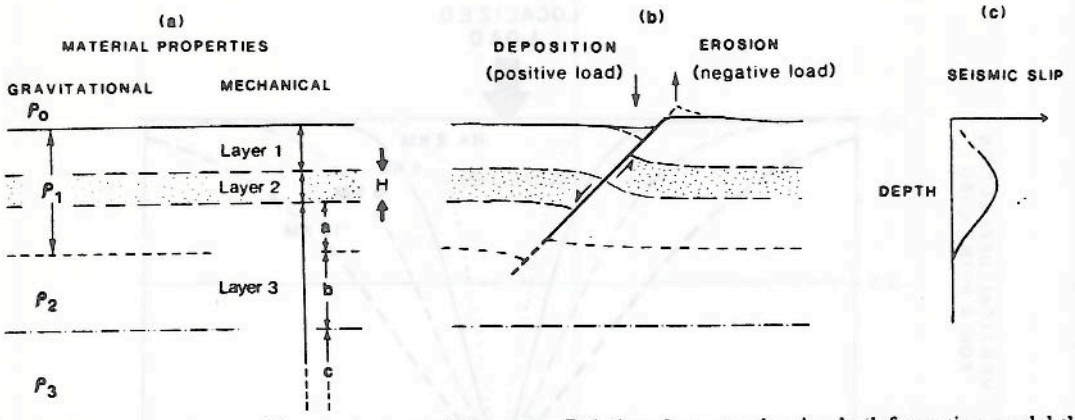

Fig. 5. Parameters that could control crustal deformation.Relations between the simple deformation model that we adopt and more elaborate models represented by Figures 5*a* and 5*b* are discussed in the text. A typical depth distribution of seismic slip is shown in Figure 5*c* [e.g., *Bakun* et al., 1986].

Starting from the bottom, layer 3 behaves in an elastic-brittle fashion during earthquakes, but over longer time periods is ductile. Layer 2 behaves in an elastic-brittle manner and is the only part of the crust that has substantial long-term strength. If all the long term strength resided in it alone, it would have a thickness of H. Layer 1 is modelled to have similar properties to layer 3. Layer 1 cannot be truly ductile, however, or topography would disappear, although stress may be partly relieved [e.g., *King and Brewer*, 1983]. Thus deviatoric stresses can be adequate to maintain topography but remain well below the stresses required for brittle failure. The material can be thought of as having properties similar to those of a standard linear solid [e.g., *Fung*, 1965]. We therefore treat layer 1 as being capable of sustaining only limited loads and to behave such that: a load placed at the top of layer 1 has the same effect as the same load acting at the base of layer 1, and a vertical displacement at the top of the layer is equal to the vertical displacement at the bottom of the layer immediately below.

Layer 3 includes two density changes (Figure 5). Whether these changes are significant in modeling depends on if layer 3 behaves entirely or only partly as a fluid. If it were truly fluid, then these interfaces would always equilibriate to horizontal surfaces and have no effect on the deformation field in layer 2 and above. This behavior seems likely for the *b-c* interface because temperatures at mid crustal depths are sufficient to activate thermal creep processes [e.g., *Ashby and Verrall*, 1977; *Sibson*, 1982] and allow substantial stress relief. The possibility that an interface closer to the base of layer 3 becomes deformed is greater if the upper part of layer 3 behaves in a manner similar to layer 1. We do not consider this possibility. Rather, we consider layer 3*a* to be of zero thickness and layer 3b to extend infinitely downward. Since density differences at the deeper interfaces are small, they contribute no more than a few percent to changes in the gravity potential and thus little to the deformation. We use a mantle density for this lower layer, although we recognize that in some cases this choice can cause loading flexure to be underestimated (see Table 1).

FLEXURE DUE TO EROSION AND DEPOSITION

The effect of sedimentation and erosion can be treated as a set of positive and negative loads acting at the top (and thus the bottom) of layer 1. We treat layer 2 as a thin plate. The added complexity of considering a plate of finite thickness [e.g., *McKenzie and Bowin*, 1976] does not seem justified for the cases that we consider (see *Rundle*, [1982*b*] and *Comer*, [1983] for discussions).

Expressions for a two-dimensional (line load) are provided by *Gunn* [1943] and are reproduced by *McNutt* [1980]. To model flexure, we approximate sediment deposition and erosion by a series of loads F and sum together the deflections calculated from the following expression:

$$w = e^{-kx} \frac{Fk}{2\Delta\rho g} \left(\cos|kx| + \sin|kx|\right) \quad (1)$$

where the flexural rigidity of the crust D is given by

$$D = \frac{E H^3}{12\left(1-\nu^2\right)} \quad (2)$$

and the wave number of the deformation, k, is related to other constants by

$$k^4 = \frac{4D}{\Delta\rho g} \quad (3)$$

TABLE 1. Modeling Constants

Variable	Definition	Value
E	Young's Modulus	2.5×10^{10} N m^{-2}
ρ_o	Atmospheric Density	0.0×10^{3} kg m^{-3}
ρ_s	Sediment Density	2.7×10^{3} kg m^{-3}
ρ_1	Upper Crustal Density	3.0×10^{3} kg m^{-3}
ρ_2	Lower Crustal Density	3.5×10^{3} kg m^{-3}
ν	Poisson's Ratio	0.25

Density layers are illustrated in Figure 5.

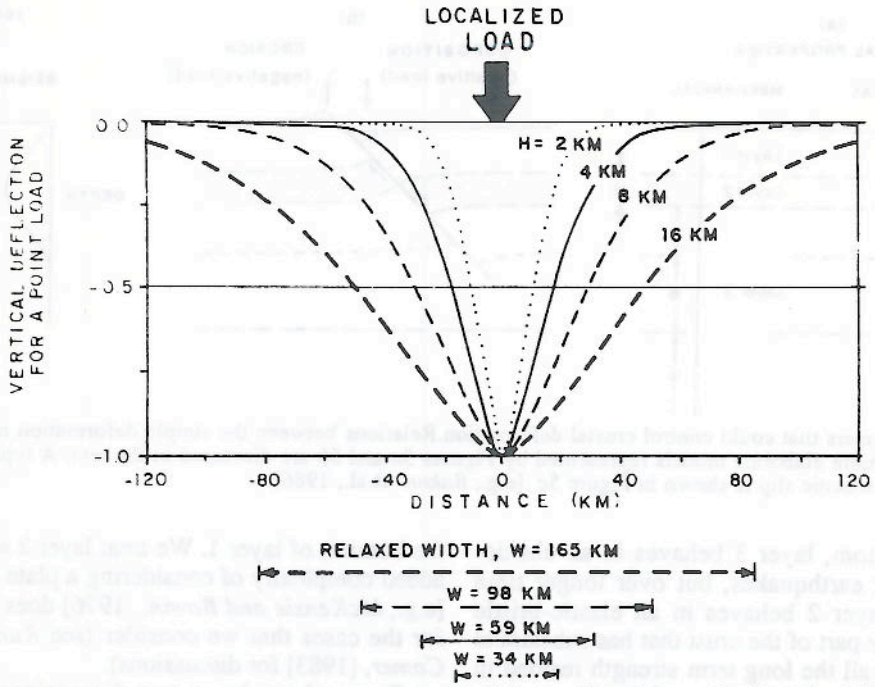

Fig. 6. Surface deformation of a gravitating plate overlying a fluid medium due to a localized load. Deformation distributions are normalized to constant maximum displacement. The width (W) corresponds to where the deformation amplitudes drop to 20% of the maximum displacement.

The plate has a thickness H and an elastic modulus E. The difference in density between the fluid beneath the plate and the air above we term $\Delta\rho$. Referring to Figure 5, $\Delta\rho = \rho_2 - \rho_1$. The x axis is horizontal and the load acts at x=0. The plate corresponds to layer 2 and the fluid to layer 3, in Figure 5. Recall that deflections at the top of layer 1 are considered adequately represented by those at the base.

From these expressions it can be seen that plate deflection is inversely proportional to the fourth root of flexural rigidity of the plate and the wavelength of the deflection is nearly inversely proportional to the plate thickness. Combining (1), (2), and (3) and evaluating the surface displacement at x=0,

$$w_{(0)} = \frac{2}{3} \frac{F}{(H\Delta\rho g)^{3/4} E^{1/4}} \tag{4}$$

The displacement is thus linearly dependent on the load, depends modestly on the plate thickness and the density contrast and is insensitive to the modulus E.

The expression for vertical displacements due to a point load is also straightforward [e.g., *Lambeck and Nakiboglu*, 1980]:

$$w = \frac{-Fl^2}{2\pi D} kei\left(\frac{r}{l}\right) \tag{5}$$

where

$$l^4 = \frac{D}{\Delta\rho g}$$

r is the radial distance from the load, and *kei* (x) is the zero-order Kelvin function. Equation (5) is evaluated numerically [e.g., *Abramowitz and Stegun*, 1972].

The deflection due to a localized load as a function of radial distance is shown for various elastic thicknesses in Figure 6. It can be seen that for a 16-km-thick layer, the width is about 165 km; for a 2 km thick layer, the width is 34 km. The area under the curves outside these regions is about 5% of the total area. Thus localized loads at half these distance ranges would have to be very large to cause even a 5% error in a two-dimensional approximation of a structure. Even at a fourth of the distances, 20% errors would result only if the loads deviated by 100% from the assumption of constant behavior along strike. A satisfactory rule that determines the range of validity of later figures is that two-dimensional models are accurate within a few percent provided that the length of the structure is about 10 times the effective elastic thickness. Tests of both the dislocation program and the loading program for a set of structures of finite extent were used to independently confirm this conclusion.

IDEALIZED STRUCTURES

We now combine the relaxed deformation and the deflection caused by surface loads, as shown schematically in Figure 1 to illustrate the influence of effective elastic thickness and erosion and deposition of sediment. Note that we only calculate vertical and not horizontal components of displacement, and thereby introduce some error in the form of the figures. However we display the results at 20:1 vertical exaggeration and since the horizontal displacements have about the same amplitude as the vertical displacements, apparent errors in the figures due to this simplification do not exceed 5%. Both the dislocation and the loading models are strictly appropriate only when the elastic strains are small. Because the elastic parts are in the form of thin plates even the large displacements that we show do not violate the small strain assumption.

The effect of varying elastic thickness for a series of

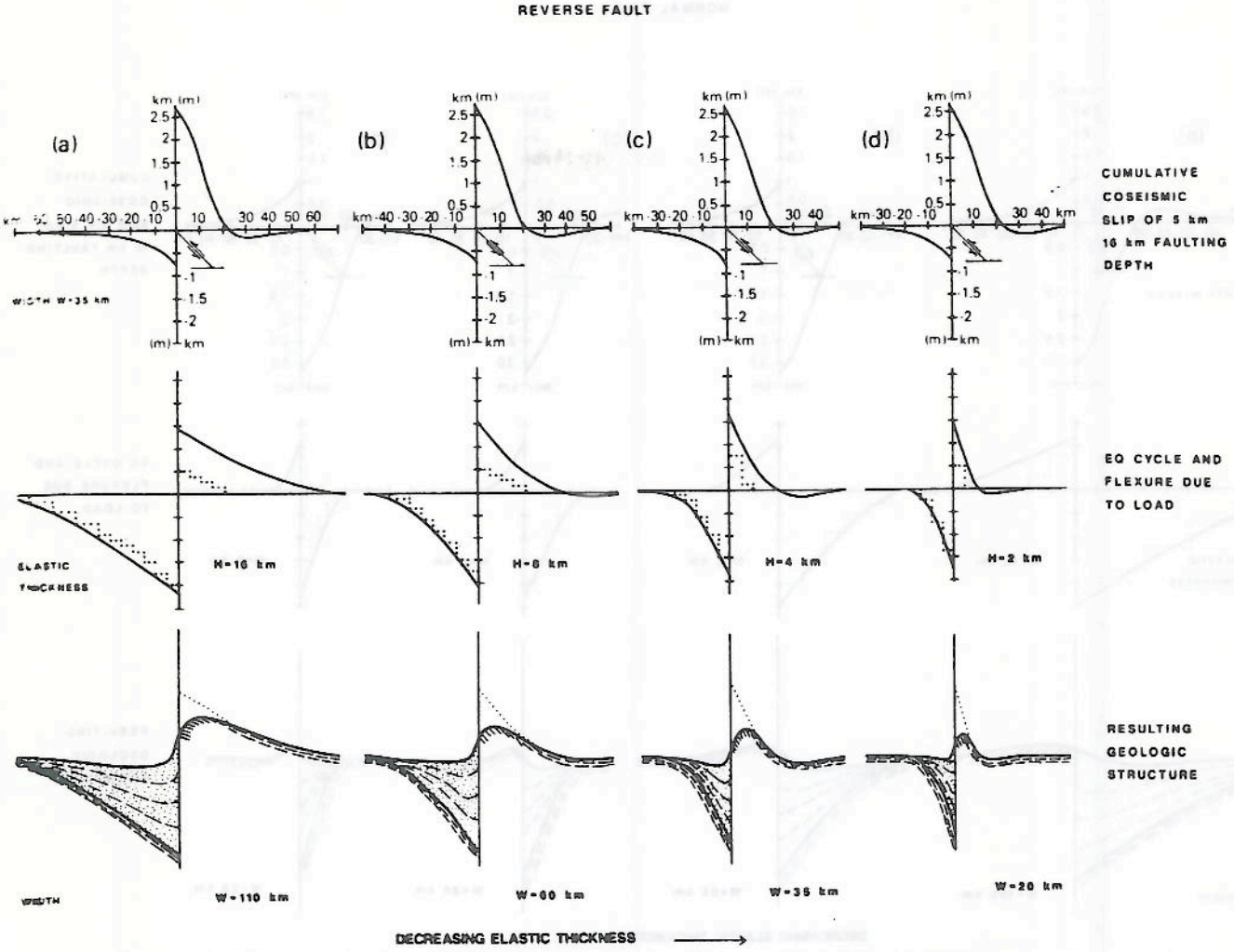

Fig. 7. The influence of flexural rigidity on vertical displacements associated with reverse faulting. The upper figures show coseismic displacement for a fault extending to a depth of 16 km. The middle figures show vertical displacements when stress is relaxed at various depths. Loads to account for erosion and deposition are added. Elastic thicknesses (H) are, from left to right 16, 8, 4, and 2 km. The deformation with loading is shown in the middle row and the loads used in each case are shown as dotted histograms. The lower figures indicate the type of structure represented by the middle figures. Assumptions used to construct these cross sections are discussed in the text.

reverse faults is shown in Figure 7. The upper row of figures are identical and show the coseismic displacement for a fault extending to a depth of 16 km. The middle figures show, with a solid line, the relaxed deformation summed with the deformation due to the load. The relaxed deformation profiles are for layer thicknesses of 16, 8, 4, and 2 km (Figures 7*a*-7*d*). The loads used to calculate the deformation (dotted histograms) represent depths of sediment measured downwards from the horizontal axes (positive loads) or depth of erosion when measured upward (negative loads). The form of the loads has been chosen such that when the histograms are smoothed and subtracted from the deformation profile, the land surfaces generated are not unreasonable. Extreme examples of unreasonable load distributions produce hills of sediment in the down thrown block or valleys cutting below the mean ground surface in the up thrown block. Less extreme examples also produce unlikely morphologies. In practice the choice of load distribution is limited. The chosen land surfaces are shown in the third row of figures. To indicate the relation of these plots to geological structures, other features have been added to the figures in the third row. The sediment includes dashed lines to indicate earlier surface profiles in the evolution of the structure; they are positioned assuming that the feature has evolved by steadily increasing its vertical exaggeration. The validity of such an assumption is discussed in *Paper 2* in the context of modeling real structures. Bedding is also shown in the material that was beneath the original undeformed land surface. Bedding lines are drawn parallel to and beneath that surface. We see from the figures that if the long-term effective elastic thickness of the crust is the same as the depth of earthquake faulting (i.e., H=16 km), then the width of the resulting structure (W=110 km) is much greater than the coseismic width (W=35 km). However, if the effective elastic thickness drops to W=4 km, then the structure width and the coseismic width become the same.

The equivalent set of figures for normal faults are shown in Figure 8, and we can draw similar conclusions about the role of effective elastic thickness. In both cases the

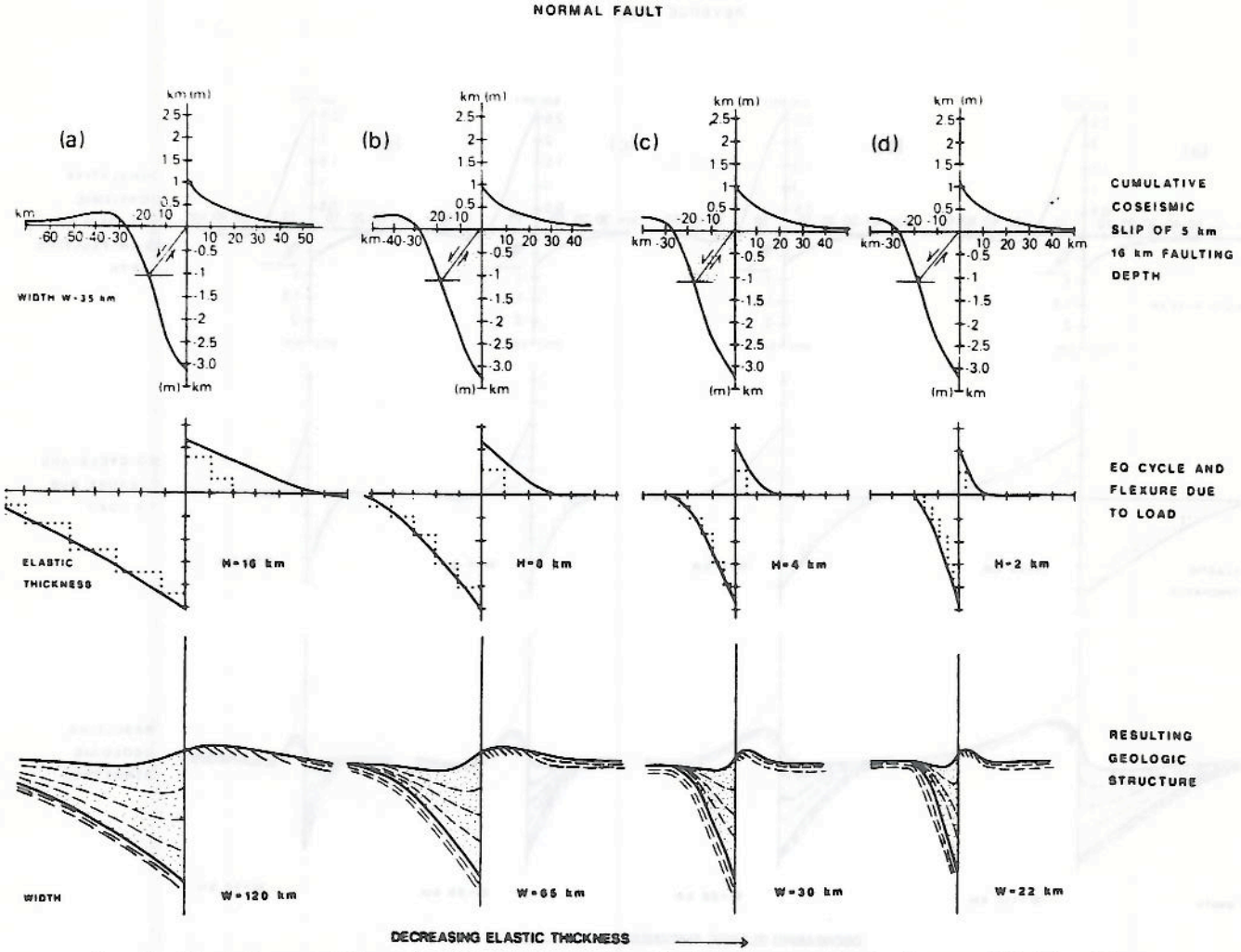

Fig. 8. The influence of flexural rigidity on the vertical displacement associated with normal faulting. Like Figure 7, the upper row is coseismic deformations, the middle row are relaxed deformation with loading, and the bottom row is representative structures. Note that for similar load conditions, reverse and normal faults result in structures of similar width.

examples illustrate that the structure widths (W) depend on the effective elastic thickness. The structures (Figures 8*a* and 8*b*) produced using effective elastic thicknesses (H) of 16 or 8 kilometers with widths (W) of 120 and 65 km respectively are much wider than structures commonly observed in the field and wider than the region of coseismic deformation. Thicknesses of 4 and 2 km (in Figures 8c and d) produce features with dimensions that resemble observed structures. We examine this in relation to specific structures in *Paper 2*, but this observation forms the basis for concluding that whatever we may believe its physical significance to be the effective elastic thickness of the crust is substantially less than the elastic depth of coseismic faulting or the depth range over which micro-earthquakes occur.

The effect of changes in the amount of erosion and sedimentation on the form of the resulting structures is illustrated in Figures 9 and 10. Again the upper plots show the coseismic deformation for a fault extending to a depth of 16 km. In the second row the relaxed deformation is shown for a 4 km effective elastic thickness but the net cross-sectional area of the load (A= [depositional load]-[erosional load]) increases from left to right; from 1 km^2 in Figure 9*a* and 2 km^2 in Figure 9*b* to 9 km^2 in Figure 9*c* for reverse faults, and from 2 km^2 in Figure 10*a* and 4.5 km^2 in Figure 10*b* to 5.5 km^2 in Figure 10*c* for normal faults. The corresponding structures are shown in the row below. It can be seen that increased loading always acts to widen the structure and never to narrow it. In Figure 9, a small basin can be seen to form in the upthrown block. Like the larger basin formed by the downthrown block, this basin can collect sediment (Figure 9*c*). For the normal faults illustrated in Figure 10, the equivalent up-arching of the downdropped footwall block is diminished in amplitude by loading in the main basin. It is very interesting that the feature which forms the basin in the hanging wall of a reverse fault has the same geometrical origin as the up-arch in the footwall of a normal fault. Both are illustrated with field examples in *Paper 2*.

DISCUSSION

Existing models can be adapted to describe the vertical deformation associated with a complete earthquake cycle,

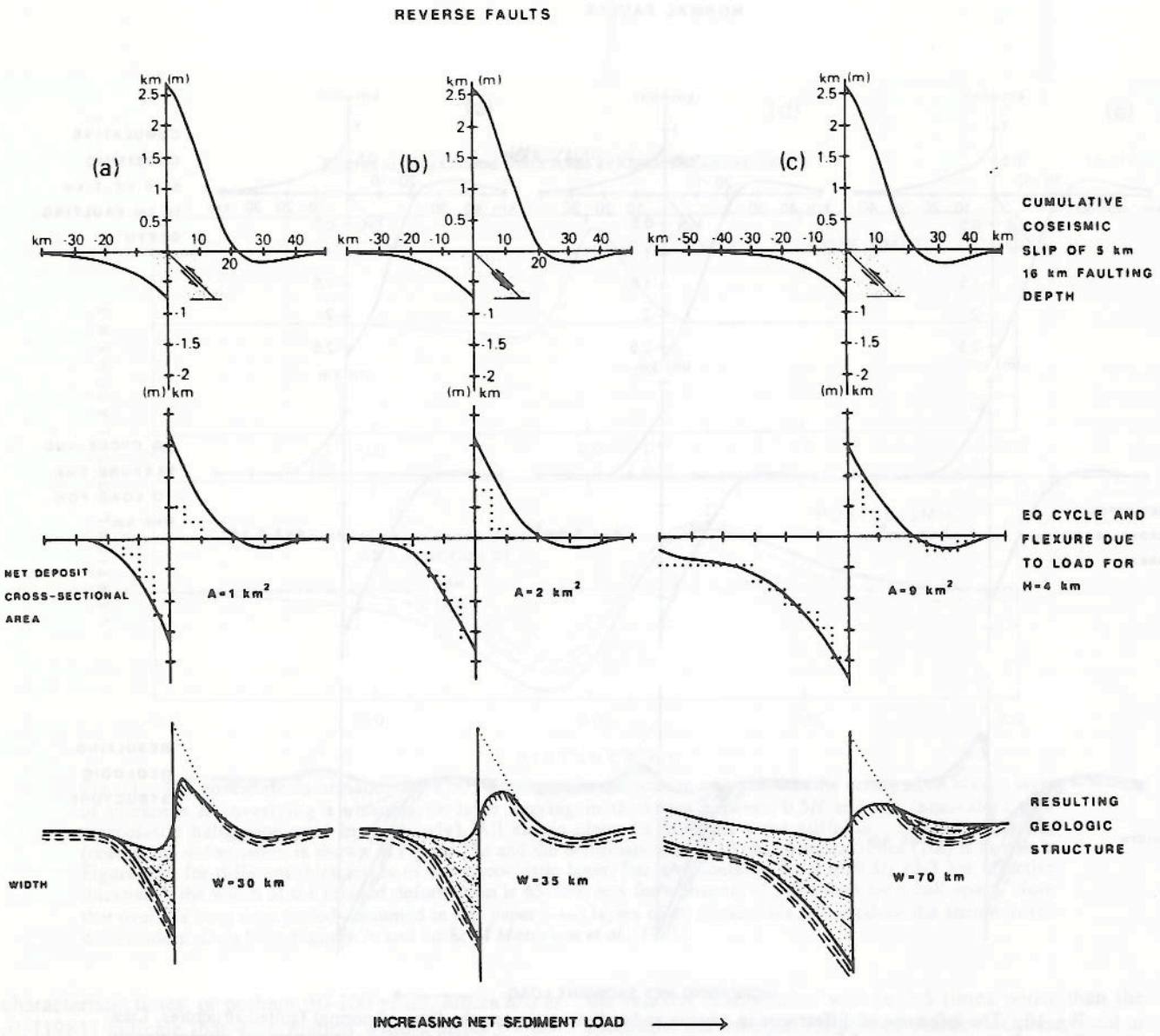

Fig. 9. The influence of differences in erosion and deposition on the form of reverse faulted structures. The upper row of figures is the coseismic vertical displacements. The middle row of figures shows the vertical displacement for a constant elastic thickness (H) of 4 km with different applied loads. Erosion and deposition increase from left to right. The cross-sectional area (A) of each load is indicated. Note that the right-hand figure corresponds to a structure, such as the White Wolf fault, associated with a large net sediment influx. Note also the dip in the vertical displacement in the hanging wall of all of the figures. The bottom row of figures indicates the structures represented by the middle row of figures. Arrows indicate hanging wall dips. In the bottom right-hand figure the hanging wall dip is filled with sediment. This structure is similar in scale and form to the those associated with the White Wolf fault (*Paper 2*).

but the effect of loading due to erosion and deposition of sediment must be considered. The complete seismic cycle takes too long for us to hope to make direct measurements except at oceanic plate boundaries; intraplate earthquakes have afforded the opportunity to measure postseismic deformation only during the first several decades after a large event [*Reilinger*, 1986]. However, we can conclude that originally horizontal geological horizons become deformed as the sum of the effects of repeating earthquakes and may be treated as if they are fossilized leveling lines that record very large displacements.

Following this view, we can produce structures that closely resemble those commonly observed in the field and in reflection profiles. Two parameters control the form of the structures. The overall width is determined by the long-term effective elastic thickness of the crust, and the asymmetry of uplift to subsidence is largely controlled by sediment loading. Loading can increase the width of a structure, but it cannot reduce it.

The form of geological structures is such that the crust commonly appears to have an effective elastic thickness of less than 4 km, even in regions where major earthquakes are known to extend to depths 4 times as great and where micro-earthquakes occur over a similar extended depth

effective elastic thickness and the load distribution, we can produce a wide range of possible structures to compare with field examples. The most reasonable structures, however, can only be generated if we assume that the effective elastic thickness is very small.

Acknowledgments. We thank the Natural Environment Research Council of Britain (GR3/3904) and the Nuffield Foundation for support during the early stages of this study. We appreciate helpful reviews by Maria Zuber, Jim Savage, Wayne Thatcher, Dave Schwartz, Jian Lin, and an anonymous reviewer.

REFERENCES

Abramowitz, M., and I. A. Stegun, *Handbook of Mathematical Functions*, 9th ed., *Dover*, New York, 1972.

Ashby, M. F., and R. A. Verrall, Micromechanisms of flow and fracture and their relevance to the rheology of the upper mantle, *Philos. Trans. R. Soc. London, Ser. A, 288*, 59-95, 1977.

Bakun, W. H., G. C. P. King and R. Cockerham, Seismic slip, aseismic slip, and the mechanics of repeating earthquakes on the Calaveras fault, California, *Earthquake Source Mechanics, Geophys. Mongv. Sev.* 37, (Maurice Ewing 6), edited by S. Sas, J. Boatwright, and C. H. Scholz, pp. 195-207, AGU, Washington D.C., 1986.

Bills, B. G., and G. M. May, Lake Bonneville: Constraints on lithospheric thickness and upper mantle viscosity from isostatic warping of Bonneville, Provo, and Gilbert stage shorelines, *J. Geophys. Res., 92*, 11,493-11,508, 1987.

Cochran, J. R., Some remarks on isostasy and the long-term behavior of the continental lithosphere, *Earth Planet. Sci. Lett., 46*, 266-274, 1980.

Cohen, C. C., and M. J. Kramer, Crustal deformation, the earthquake cycle, and models of visco-elastic flow in the asthenosphere, *Geophys. J. R. Astron. Soc., 78*, 735-750, 1984.

Comer, R. P., Thick plate flexure, *Geophys. J. R. Astron. Soc., 72*, 101-113, 1983.

Forsyth, D. W., Subsurface loading and estimates of the flexural rigidity of the continental lithosphere, *J. Geophys. Res., 90*, 12623-12632, 1985.

Fung, Y. C., *Foundations of solid mechanics*, Prentice-Hall, Engelwood Cliffs, N. J., 525 p., 1965.

Gunn, R., A quantitative study of isobaric equilibruim and gravity anomalies in the Hawaiian Islands, *J. Franklin Inst., 238*, 373-396, 1943.

King, G. C. P., and J. Brewer, Fault related folding near the Wind River thrust, Wyoming, U.S.A., *Nature, 306*, 147-150, 1983.

Lambeck, K., and S. N. Nakiboglu, Seamount loading and stress in the ocean lithosphere, *J. Geophys. Res., 85*, 6403-6418, 1980.

Matsu'ura, M.,T. Tanimoto, and T. Iwasaki, Quasi-static displacements due to faulting in a layered half-space with an intervenient visco-elastic layer, *J. Phys. Earth, 29*, 23-54, 1981.

McKenzie, D. P., and C. Bowin, The relationship between bathymetry and gravity in the Atlantic Ocean, *J. Geophys. Res., 81*, 1903-1915, 1976.

McNutt, M., Implications of regional gravity for the state of stress in the earth's crust and upper mantle, *J. Geophys. Res., 85*, 6377-6396, 1980.

Reid, H. F., The mechanics of the earthquake, The California Earthquake of April 18, 1906: Report of the State Earthquake Investigation Commission, vol.2, Publ. 87, Carnegie Inst. of Wash., Washington, D.C., 1910.

Reilinger, R. E., Evidence for postseismic viscoelastic relaxation following the 1959 M=7.5 Hebgen Lake, Montana earthquake, *J. Geophys. Res., 91*, 9488-9494, 1986.

Rundle, J. B., Static elastic-gravitational deformation of a layered half-space by point couple stresses, *J. Geophys. Res., 85*, 5355-5363, 1980.

Rundle, J. B., Vertical displacements from a rectangular thrust fault in a layered elastic-gravitational earth, *J. Phys. Earth, 29*, 173-186, 1981.

Rundle, J. B., Viscoelastic-gravitational deformation by a rectangular thrust fault in a layered earth, *J. Geophys. Res., 87*, 7787-7796, 1982a.

Rundle, J. B., Deformation, gravity and potential change due to volcanic loading of the crust, *J. Geophys. Res.* 87, 20,729-10,744, 1982*b*. (Correction, *J. Geophys. Res., 88*, 10,647-10,652, 1983.)

Savage, J. C., and G. Gu, A plate flexure approximation to postseismic and interseismic deformation, *J. Geophys. Res., 90*, 8570-8580, 1985.

Sibson, R. H., Fault zone models, heat flow, and the depth distribution of earthquakes in the continental crust of the United States, *Bull. Seismol. Soc. Am.,72*, 151-163, 1982.

Stein, R. S., G. C. P. King, and J. B. Rundle, The growth of geological structures by repeated earthquakes 2, Field examples of continental dip-slip faults, *J. Geophys. Res.*, this issue.

Stein, R.S, and G.C.P. King, Seismic potential revealed by surface folding: the 1983, Coalinga, California, Earthquake, *Science, 224*, 869-872, 1984.

Thatcher, W., The earthquake deformation cycle at the Nankai Trough, southwest Japan, *J. Geophys. Res., 89*, 3087-3101, 1984.

Thatcher, W., and J. B. Rundle, A model for the earthquake cycle in underthrust zones, *J. Geophys. Res., 84*, 5540-5556, 1979.

Vita-Finzi C., and G.C P. King, The seismicity, geomorphology and structural evolution of the Corinth area of Greece, *Philos. Trans. R. Soc. London Ser. A, 314*, 379-406, 1984.

Wallace, R.E., Pattern and timing of Late Quaternary faulting in the Great Basin province and its relation to some regional tectonic features, *J. Geophys. Res., 89*, 5763-5769, 1984.

Watts, A. B., C. O. Karner, and M. J. Steckler, Lithospheric flexure and the evolution of sedimentary basins, *Phil. Trans. R. Soc. London, Ser. A, 305*, 249-281, 1982.

G. C. P. King, U.S. Geological Survey, Box 25046, MS 966, Denver Federal Center, Denver, CO 80225

J. B. Rundle, Division 5541, Sandia National Laboratories, Albuquerque, NM 87185.

R. S. Stein, U.S. Geological Survey, 345 Middlefield Road, MS 977, Menlo Park, CA 94025.

(Received December 21, 1987:
revised May 24, 1988:
accepted July 1, 1988)